SPECTRAL-SPATIAL MINERAL CLASSIFICATION USING EDS X-RAY IMAGES: APPLICATION TO SHERGOTTITES. Matthew R. M. Izawa[1] and Brendon J. Hall[2], [1]Institute for Planetary Materials, Okayama University, Misasa, Tottori, 682-0193, Japan (matthew.izawa@gmail.com), [2]Enthought Inc., 515 Congress Avenue, Suite 2100, Austin TX 78701 USA (bhall@enthought.com).

Introduction: Modern instrumentation allows the collection of very large data volumes of chemical microanalytical data in the form of X-ray chemical maps using scanning electron microscopes equipped for energy dispersive X-ray spectroscopy (EDS). A typical EDS data set for a petrographic thin section might produce ten or more images of several mB, imaging an area of a few cm^2 at a resolution of a few μm/pixel. Thus, it is rapidly becoming practically impossible for a human investigator to carefully examine the full data set. Reliable classification can form the basis of further qualitative and quantitative analyses, and provides useful insights when the classes can be assigned physical meaning (e.g., in terms of minerals).

Sample Description: Northwest Africa 7257 is an enriched shergottite consisting dominantly of elongate euhedral to subhedral pyroxene laths (containing a mixture of pigeonite, augite, and ferropigeonite) with interstitial plagioclase (Table 1). Accessory phases include ilmenite, Fe-Cr-Ti spinel, pyrrhotite, chlorapatite, merrillite, K-rich melt pockets, and rare baddeleyite and fayalite [1].

EDS Image Acquisition: Backscattered electron (BSE) imagery and EDS X-ray spectra were acquired for a polished thin section of NWA 7257 using a JEOL JSM-7001F scanning electron microscope with Oxford X-max detector. The X-ray spectra were sampled to produce images which map the intensity of individual elements (Al, C, Ca, Cl, Cr, Fe, K, Mg, Mn, Na, O, P, S, Si, Ti, Zr).

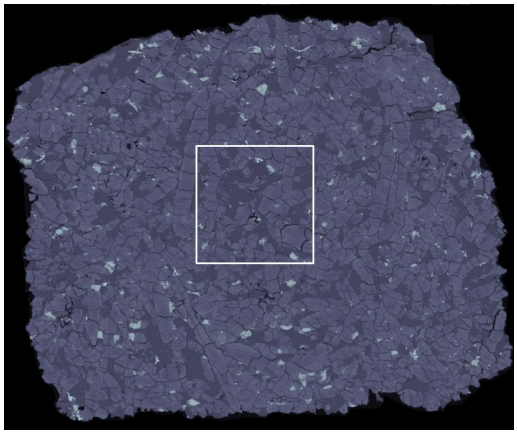

Figure 1: BSE image of the NWA 7257 thin section. The entire image is 820×690 px. The 200×200 px subregion used in this study is indicated by the white square.

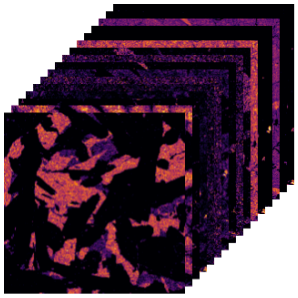

Figure 2: EDS image set of the 200x200 px subregion. The first image is the series is the aluminum (Al) map.

Image Classification: Tarabalka et al. [2] proposed a spectral-spatial approach for classifying hyperspectral satellite images. A flowchart of the algorithm is shown in Figure 2. The BSE and EDS images provide N=17 (1 BSE and 16 EDS) features at each pixel location. The classification task consists of assigning one of k classes to each pixel based on its features. A training set is created by manually assigning representative pixels from each class. The BSE-EDS feature set and training points provide the input to the spectral-spatial classification algorithm.

Spectral Classification. The initial step uses a support vector machine (SVM) to perform a probabilistic classification for every pixel in the image. [3] The SVM learns from the training data by dividing the N dimensional feature space into k sub-regions by maximizing the margins between the classes. Each pixel of the image is mapped to one of the k sub-regions to obtain the spectral classification map (Figure 4, middle pane). Class probabilities are determined using Platt scaling [4].

Spatial Regularization. The spectral classification considers only the information available at each pixel location. Most structures in the image are larger than one pixel. The SVM does not take the spatial structure of the data into account, which can result in a noisy classification map. A Markov Random Field (MRF) regularization step is used to smooth the result. This approach is based on the assumption that a pixel belonging to a given class is likely to be surrounded by pixels having the same class. The regularization is formulated as the minimization of a suitable energy function. The energy function has a spectral component and a spatial component. The local energy of a given pixel x_i is:

$$U(x_i) = U_{spectral}(x_i) + U_{spatial}(x_i) \quad (1)$$

The spectral energy term is

$$U_{spectral}(x_i) = -lnP(x_i|L_i) \quad (2)$$

where $P(x_i|L_i)$ are the class probabilities found by the SVM. The spatial energy is found by comparing the class of a pixel with the class of neighboring pixels. For pixel x_i, let N denote the set of 8 immediately neighboring pixels. The spatial energy is calculated by

$$U_{spatial}(x_i) = \sum_{x_j \varepsilon N_j} \beta(1-\delta(L_i, L_j)) \quad (3)$$

where δ is the Kronecker delta function and β is a parameter that controls the relative importance of the spectral vs. spatial energy terms. Equation (1) is minimized using a version of the Metropolis algorithm [5].

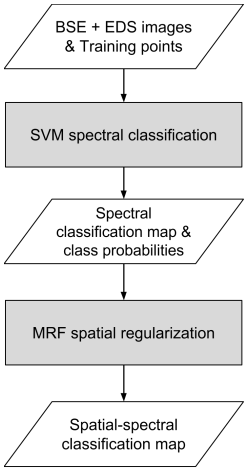

Figure 3: Workflow of the SVM-MRF classification algorithm.

Results: The classification results are shown in Figure 4. The left pane shows the BSE image for comparison. The middle pane contains the spectral classification map. The results are quite noisy, especially between zoned phases such as pigeonite and ferropigeonite. The right pane shows the MRF regulated classification map, showing the reduction in isolated unclassified pixels. The final result clearly distinguishes many key petrographic features including the pigeonite cores of pyroxene laths, complex augite and ferropigeonite overgrowths, and interstitial maskelynite and melt. Abundances from each phase can be calculated and are shown in Table 1.

Discussion: The image classifier algorithm tested here has demonstrated the ability to correctly classify minerals including those with complex crystal chemical variations (pyroxene, spinel) and minor phases. This is an important first step towards goals such as intelligent systems that can rapidly assess a high-resolution SEM image data set to find interesting regions (to flag for human investigation), and to integrate chemical microanalysis with textural parameters and petrographic context (e.g., what sets minerals are close to or in contact with each other).

References: [1] Irving A. J. et al., (2012) *75th Meteoritical Society Meeting* [2] Tarabalka, Y. et al. (2010) *IEEE Geoscience and Remote Sensing Letters, 7(4),* 736–740. [3] Pedregosa, F. et al. (2011) *JMLR 12,* 2825–2830. [4] Lin H. T. et al. (2002) *Mach. Learn.,* 68(3), 267–276. [5] Metropolis, A. et al. (1953) *J. Chem. Phys.,* 21(6) 1087–1092.

Mineral	Formula/elements	Abundance (%)
Augite	$(Ca,Na)(Mg,Fe,Al)(Al,Si)_2O_6$	6.5
Ferro-pigeonite	$(Mg,Fe,Ca)SiO_3$, Fe-rich	18.5
Pigeonite	$(Mg,Fe,Ca)SiO_3$	37
Maskelynite	$(Ca,Na)(Al,Si)AlSi_2O_8$	22.2
Melt	elevated Si and K	7.1
Ilmenite	$FeTiO_3$	1.2
Chlorapatite	$Ca_5(PO_4)_3(Cl)$	0.06
Merrillite	$Ca_9NaMg(PO_4)_7$	4.2
Pyrrhotite	$Fe_{1-x}S$	0.5

Table 1: Mineral classes, formula and abundances from spectral-spatial classification result.

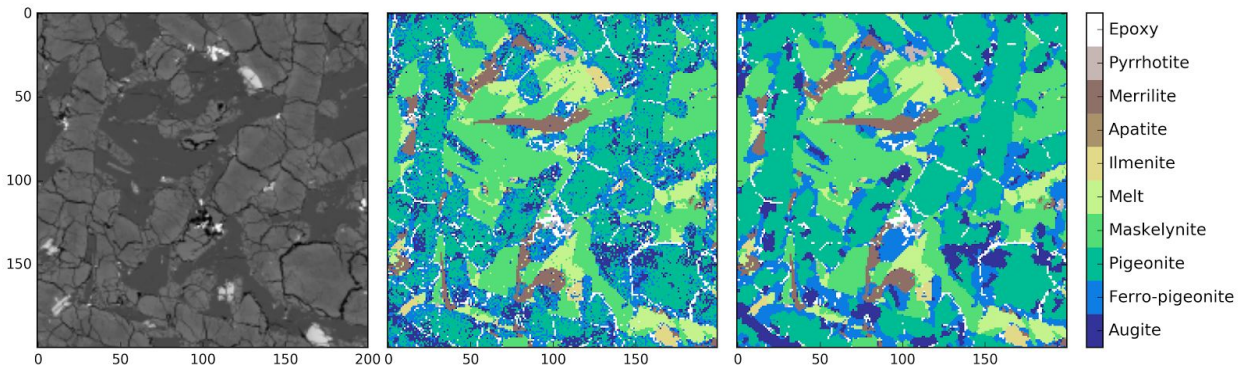

Figure 4: Results of the SVM-MRF classification. The left pane shows the BSE image from the 200×200 px subregion for comparison. The middle pane contains the spectral classification map. The right pane contains the spectral-spatial classification result.